



Available online at <http://scik.org>

J. Math. Comput. Sci. 2022, 12:8

<https://doi.org/10.28919/jmcs/6624>

ISSN: 1927-5307

# MIXTURE OF $Al_2O_3$ -Cu/ $H_2O$ -( $CH_2OH$ ) $_2$ MHD HYBRID NANOFLUID FLOW DUE TO A STRETCHABLE ROTATING DISKS SYSTEM UNDER THE INFLUENCE OF NON-UNIFORM HEAT SOURCE OR SINK AND THERMAL RADIATION

OGUNSOLA AMOS WALE, AKINDELE AKINTAYO OLADIMEJI\*

Department of Pure and Applied Mathematics, Ladoké Akintola University of Technology, Ogbomoso, Nigeria

Copyright © 2022 the author(s). This is an open access article distributed under the Creative Commons Attribution License, which permits unrestricted use, distribution, and reproduction in any medium, provided the original work is properly cited.

**Abstract:** This paper investigates the theoretical analysis of hybrid nanofluid flow due to stretchable rotating disks system under the influence of non-uniform heat source or sink and thermal radiation. Two types of nanoparticles Copper (Cu) and Alumina ( $Al_2O_3$ ) mixed with the base fluid (ethylene glycol and water) in a ratio 50:50 were considered. The governing partial differential equations were considered in a cylindrical coordinate and Von Karman transformations were rendered into the system to obtain equivalent Ordinary differential equations. The resulting non-linear Ordinary differential equations together with their initial and boundary conditions were solved using finite differences method (FDM) with the aid of maple 18.0 software. The numerical result obtained shows the effect of Reynolds number, Radiation parameter, magnetic parameter and volume fraction of hybrid nanoparticles on the total Entropy generation and Bejan number. Also, the Skin friction Coefficient and Nusselt number at the lower and upper rotating disk were examined for different parameters and the effects of various parameters on the Axial, radial and tangential velocities and the thermal field presented graphically.

**Keywords:** hybrid nanoparticle; ethylene glycol; thermal radiation; volume fraction; stretchable rotating disks.

**2010 AMS Subject Classification:** 35Q92.

---

\*Corresponding author

E-mail address: [aoakindele65@pgshcool.lautech.edu.ng](mailto:aoakindele65@pgshcool.lautech.edu.ng)

Received August 10, 2021

## 1. INTRODUCTION

The use of copper as nanoparticle suspended in the base fluid have received a lot of attention in the recent decades due to its extraordinary performance as antibacterial and antimicrobial agents as well as its heat conduction activities. Majzlik *et al.* [1]. Its application in industries such as pharmaceuticals, food, aeronautic, cosmetics, electronics and environmental science cannot be over-emphasized.

Rotating disk with hydrodynamic flow was first investigated in the year 1921 by Von Kanman [2], in his work which introduced a similarity transformation that was later adopted by many researchers. Magnetohydrodynamic (MHD) flow of Cu-water nanofluid due to a rotating disk with partial slip was studied by Hayat *et al.* [3]. Zangoee *et al.* [4] considered hydrothermal analysis of MHD nanofluid (TiO<sub>2</sub>-GO) flow between two radiative stretchable rotating disks using AGM. Chaoli Zhang *et al.* [5] studied MHD flow and radiation heat transfer of nanofluids in porous media with variable surface heat flux and chemical reaction. Nanofluid flow and heat transfer due to a rotating disk was studied by Mustafa Turkyilmazoglu [6]. Mushtaq and Mustafa [7] studied the computations for nanofluid flow near a stretchable rotating disk with axial magnetic field and convective conditions. Recently, Akindele and Ogunsola [8] analyzed the study of non-isothermal permeable flow of nano-fluids in a stretchable rotating disk system. Vimal Kumar Joshi *et al.* [9] analytically discussed the numerical investigation of magnetic nanofluids flow over rotating disk embedded in a porous medium. MHD fluid flow and heat transfer due to stretchable rotating disk was investigated by Mustafa [10]. The researchers [11-29] presented their valuable contributions on the flow of nanofluids in a rotating disks system.

Recent researches on nanotechnology as proven that hybrid nanoparticles are more effective compare to ordinary nanoparticles. Hybrid nanoparticles are prepared by suspending different types of nanoparticules (more than one) in the base fluid.

Scholars that have worked on hybrid nanoparticles are as follows: Mabood *et al.* [30] investigated Cu–Al<sub>2</sub>O<sub>3</sub>–H<sub>2</sub>O hybrid nanofluid flow with melting heat transfer, irreversibility analysis and nonlinear thermal radiation. Siddiqui *et al.* [31] carried out on trade-off for dispersion stability and thermal transport of Cu-Al<sub>2</sub>O<sub>3</sub> hybrid nanofluid for various mixing ratios.

Investigation on thermophysical properties of  $\text{TiO}_2\text{-Cu/H}_2\text{O}$  hybrid nanofluid transport dependent on shape factor in MHD stagnation point flow was considered by Ghadikolaei *et al.* [32]. Flow of hybrid nanofluid across a permeable longitudinal moving fin along with thermal radiation and natural convection was studied by Gireesha *et al.* [33]. Waini *et al.* [34] reviewed MHD flow and heat transfer of a hybrid nanofluid past a permeable stretching/shrinking wedge. Khan *et al.* [35] discussed Darcy-Forchheimer hybrid ( $\text{MoS}_2$ ,  $\text{SiO}_2$ ) nanofluid flow with entropy generation. The Study of Two-Phase Newtonian Nanofluid Flow Hybrid with Hafnium Particles under the Effects of slip was explored by Ellahi *et al.* [36]. Waini *et al.* [37] performed Hybrid nanofluid flow past a permeable moving thin needle. Aladdin *et al.* [38] carried out  $\text{Cu-Al}_2\text{O}_3/\text{water}$  hybrid nanofluid flow over a permeable moving surface in presence of hydromagnetic and suction effects. Tayebi and Chamkha [39] studied the natural convection enhancement in an eccentric horizontal cylindrical annulus using hybrid nanofluids. Free convection enhancement in an annulus between horizontal confocal elliptical cylinders using hybrid nanofluids was performed by Tayebi and Chamkha [40]. Gorla *et al.* [41] discussed heat source/sink effects on a hybrid nanofluid-filled porous cavity. Chamkha *et al.* [42] analyzed the numerical analysis of unsteady conjugate natural convection of hybrid water-based nanofluid in a semicircular cavity. Transpiration and Viscous Dissipation Effects on Entropy Generation in Hybrid Nanofluid Flow over a Nonlinear Radially Stretching Disk was examined by Farooq *et al.* [43]. Afridi *et al.* [44] carried out the Entropy Generation in  $\text{Cu-Al}_2\text{O}_3\text{-H}_2\text{O}$  Hybrid Nanofluid Flow over a Curved Surface with Thermal Dissipation. Khan *et al.* [45] carried out Computational analysis of nanofluid and hybrid nanofluid in Darcy's squeezing flow with entropy optimization. Magneto rotating flow of hybrid nanofluid with entropy generation was discussed by Khan *et al.* [46]. Sadaf and Abdelsalam [47] worked on the adverse effects of a hybrid nanofluid in a wavy non-uniform annulus with convective boundary conditions. Mixed convective slip flow of hybrid nanofluid (MWCNTs + Cu + Water), nanofluid (MWCNTs + Water) and base fluid (Water) was comparatively investigated by Mahammad *et al.* [48].

Zainala *et al.* [49] worked on MHD mixed convection stagnation point flow of a hybrid nanofluid past a vertical flat plate with convective boundary condition. Venkateswarlu and Narayana [50] investigated  $\text{Cu}_2\text{Al}_2\text{O}_3/\text{H}_2\text{O}$  hybrid nanofluid flow past a porous stretching sheet

due to temperature dependent viscosity and viscous dissipation. Roy *et al.* [51] considered Heat transfer of a hybrid nanofluid past a circular cylinder in the presence of thermal radiation and viscous dissipation. Heat transfer analysis of Cu–Al<sub>2</sub>O<sub>3</sub> hybrid nanofluid with heat flux and viscous dissipation was investigated by Ali *et al.* [52]. Aly and Pop [53] explored MHD flow and heat transfer near stagnation point over a stretching/shrinking surface with partial slip and viscous dissipation: Hybrid nanofluid versus nanofluid. Acharya *et al.* [54] worked on the hydrothermal features of magnetized TiO<sub>2</sub>–CoFe<sub>2</sub>O<sub>4</sub> water-based steady hybrid nanofluid flow over a radiative revolving disk. Cu-Al<sub>2</sub>O<sub>3</sub>/Water hybrid nanofluid through a permeable surface in the presence of nonlinear radiation and variable thermal conductivity via LSM was examined by Usman *et al.* [55]. There are some latest explorations about the hybrid nanofluid as presented in the references [56-93]. Sachin Shaw [94] explained the Impact of Cattaneo-Christov heat flux on Al<sub>2</sub>O<sub>3</sub>-Cu/H<sub>2</sub>O–(CH<sub>2</sub>OH)<sub>2</sub> hybrid nanofluid flow between two stretchable rotating disks.

The objective of the present study is to analyze the development of the Mixture of Al<sub>2</sub>O<sub>3</sub>-Cu/H<sub>2</sub>O-(CH<sub>2</sub>OH)<sub>2</sub> MHD hybrid nanofluid flow due to a stretchable rotating disks system under the influence of non-uniform heat source or sink and thermal radiation in a cylindrical coordinate. The velocities profiles, pressure profile, thermal field, skin friction coefficient, Nusselt number, total entropy generation and Bejan number are taken into consideration. The system of governing non-linear partial differential equations was transformed into their ordinary differential equations equivalents and the resulting equations were solved numerically by Newton's Finite difference technique subjected to appropriate boundary conditions.

**Nomenclature**

$(r, \theta, z)$ : Cylindrical coordinate  
 $u, v, w$ : velocity component  
 $a_1, a_2$ : lower and upper stretching rate  
 $A$ : Dimensionless radial parameter  
 $A_1, A_2$ : Scaled rate stretching parameter at the lower and upper disk  
 $B_i$ : Biot number  
 $Be$ : Bejan number  
 $Br$ : Brinkman number  
 $C_p$ : Specific heat at constant pressure (J/kg K)  
 $C_{p_{hnf}}$ : Heat capacity of hybrid nanofluid  
 $C_f$ : Skin friction coefficients  
 $Ec$ : Eckert number  
 $f_w$ : Suction/injection parameter  
 $h$ : distance  
 $M$ : magnetic parameter  
 $N_G$ : Total entropy generation  
 $K$ : Thermal conductivity  
 $k_0$ : permeability constant  
 $k^*$ : Mean absorption coefficient  
 $k_{hnf}$ : Thermal conductivity of hybrid nanofluid  
 $m$ : Exponential constant  
 $Nu$ : Nusselt number  
 $P$ : Hydrodynamic Pressure (N/m<sup>2</sup>)  
 $Pr$ : Prandtl's number  
 $q_w$ : Heat flux  
 $Q$ : Temperature dependent heat source or sink  
 $Q_1$ : Surface dependent heat source or sink  
 $Rd$ : Radative parameter  
 $Re$ : Reynolds number  
 $Re_r$ : Local Reynolds number  
 $t$ : Time

$T_1$ : Temperature of the lower disk

$T_2$ : Temperature of the upper disk

$T_\infty$ : Ambient temperature

$T_f$ : Mean temperature

$w_0$ : Suction velocity

**Greek symbols**

$\eta$ : Dimensionless parameter

$\tau$ : Rotational number

$\nu_{hnf}$ : The kinematic viscosity of hybrid nanofluid

$\alpha_{hnf}$ : Thermal diffusivity of hybrid nanofluid

$\alpha_1$ : Dimensionless temperature difference

$\beta$ : Porosity parameter

$\beta_0$ : Strength of uniform magnetic field

$\mu$ : Dynamic viscosity

$\mu_{hnf}$ : The dynamic viscosity of hybrid nanofluid

$\psi$ : Stream function

$\rho$ : Density of fluid

$\rho_f$ : Density of base fluid

$\rho_{hnf}$ : The density of hybrid nanofluid

$\sigma_{hnf}$ : Electrical conductivity of hybrid nanofluid

$\sigma_0$ : Electrical conductivity of the fluid parameter

$\sigma^*$ : Stefan-Boltzmann constant

$\varepsilon$ : Pressure constant

$\theta$ : Dimensionless temperature variable

$\Omega_1, \Omega_2$ : lower and upper rotational velocity

$\phi_1 \phi_2$ : Solid volume fraction parameter

**Subscripts**

f: Fluid

s: Solid

$nf$ : Nanofluid

$hnf$ : Hybrid nanofluid

## 2. MATHEMATICAL FORMULATION

Following [8], the flow in the gap between two stretchable rotating disks in cylindrical coordinate systems  $(r, \theta, z)$  was considered. The gap contains a fluid that is considered as a hybrid nanofluid with basefluid as a mixture of ethylene glycol ( $C_2H_6O_2$ ) and water ( $H_2O$ ) in a ratio 50:50. The upper and the lower disks are separated by distance  $h$ . The two disks rotate in an anticlockwise direction with rotational velocities  $\Omega_1$  and  $\Omega_2$ . The disks are deformable and  $a_1$  (lower) and  $a_2$  (upper) are their stretching rates. Magnetic force takes place between the two disks and the upper disk is maintained at temperature  $T_2$  and the lower disk at lesser temperature of  $T_1$ . The flow geometry is as shown on figure 1. The conservation equation for mass (continuity), radial, tangential and axial momentum and energy conservations equation models are as follows:

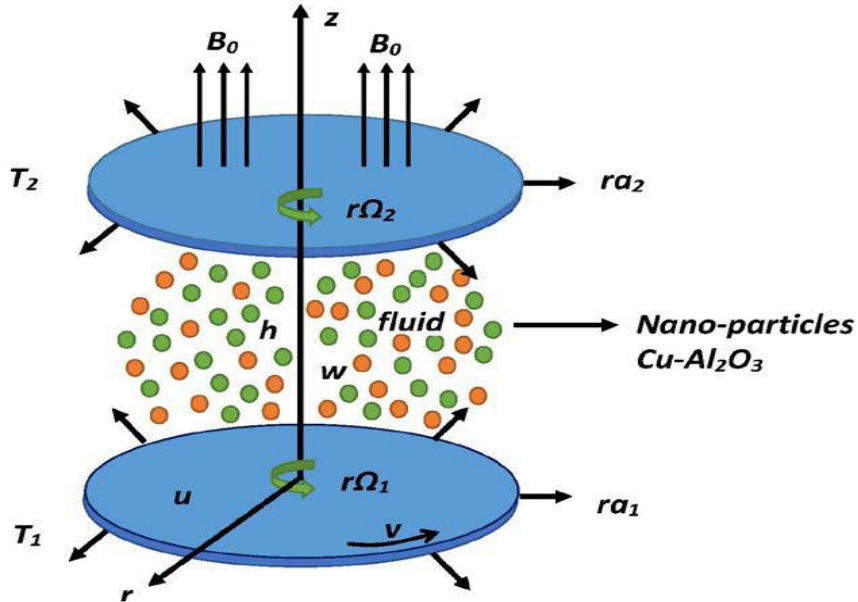


Figure 1: flow geometry between two rotating disks

(1)

$$\frac{\partial u}{\partial r} + \frac{u}{r} + \frac{\partial w}{\partial z} = 0$$

$$u \frac{\partial u}{\partial r} + w \frac{\partial u}{\partial z} - \frac{v^2}{r} = -\frac{1}{\rho_{hnf}} \frac{\partial p}{\partial r} + \frac{\mu_{hnf}}{\rho_{hnf}} \left( \frac{\partial^2 u}{\partial r^2} + \frac{1}{r} \frac{\partial u}{\partial r} + \frac{\partial^2 u}{\partial z^2} - \frac{u}{r^2} \right) - \frac{\mu_{nf}}{k_0} u - \frac{\sigma_{hnf}}{\rho_{hnf}} \beta_0^2 u \quad (2)$$

$$u \frac{\partial v}{\partial r} + w \frac{\partial v}{\partial z} + \frac{uv}{r} = \frac{\mu_{hnf}}{\rho_{hnf}} \left( \frac{\partial^2 v}{\partial r^2} + \frac{1}{r} \frac{\partial v}{\partial r} + \frac{\partial^2 v}{\partial z^2} - \frac{v}{r^2} \right) - \frac{\mu_{hnf}}{k_0} v - \frac{\sigma_{hnf}}{\rho_{hnf}} \beta_0^2 v \quad (3)$$

$$w \frac{\partial w}{\partial z} + u \frac{\partial w}{\partial r} = -\frac{1}{\rho_{hnf}} \frac{\partial p}{\partial z} + \frac{\mu_{hnf}}{\rho_{hnf}} \left( \frac{\partial^2 w}{\partial r^2} + \frac{1}{r} \frac{\partial w}{\partial r} + \frac{\partial^2 w}{\partial z^2} \right) - \frac{\mu_{hnf}}{k_0} w \quad (4)$$

$$(\rho C_p)_{hnf} \left( u \frac{\partial T}{\partial r} + w \frac{\partial T}{\partial z} \right) = \left( k_{hnf} + \frac{16\sigma^* T_2^3}{3k^*} \right) \left( \frac{\partial^2 T}{\partial r^2} + \frac{\partial^2 T}{\partial z^2} + \frac{1}{r} \frac{\partial T}{\partial r} \right) + \sigma_{hnf} \beta_0^2 (u^2 + v^2) + q''' \quad (5)$$

with initial and boundary conditions

$$\left. \begin{aligned} u = ra_1, v = r\Omega_1, w = W_0, -k_{hmf} \frac{\partial T}{\partial r} = h_f (T_f - T) \quad \text{at } z = 0 & \quad \text{(disk 1)} \\ u = ra_2, v = r\Omega_2, w = 0, T = T_2 \quad \text{at } z = h & \quad \text{(disk 2)} \end{aligned} \right\} \quad (6)$$

### 3. SIMILARITY TRANSFORMATIONS

Following [8], the Von Karman similarity transformation

is invoked using:

$$\left. \begin{aligned} u = \Omega_1 r f'(\eta), v = \Omega_1 r g(\eta), w = -2h\Omega_1 f(\eta), \\ \theta(\eta) = \frac{T - T_2}{T_1 - T_2}, \eta = \frac{z}{h}, P = \nu_f \Omega_1 \left( P(\eta) + \frac{1}{2} \frac{r^2}{h^2} \varepsilon \right) \end{aligned} \right\} \quad (7)$$

$$\text{but } q''' = (\rho C_p)_f \Omega_1 (Q(T - T_2) + Q_1(T_1 - T_2) \exp^{-\eta}) \quad (8)$$

Table.1: Thermo- physical properties of hybrid base fluid and nanoparticles [94]

Physical properties	C <sub>2</sub> H <sub>6</sub> O <sub>2</sub> -H <sub>2</sub> O (50-50)	Cu	Al <sub>2</sub> O <sub>3</sub>
$\rho \left( \frac{kg}{m^3} \right)$	1063.8	8933	3970
$C_p \left( \frac{J}{kg \cdot k} \right)$	3630	385	765
$k \left( \frac{W}{m \cdot k} \right)$	0.387	401	40
$\beta \left( \frac{1}{k} \right)$	5.8*10 <sup>-4</sup>		
$k \left( \frac{1}{m \cdot \Omega} \right)$	9.75*10 <sup>-4</sup>		

where,  $u, v, w$  are the radial, tangential, and axial velocity components in the  $(r, \theta, z)$  directions respectively.  $T$  is the temperature,  $p$  is hydrodynamic pressure of the fluid and  $\rho_{hmf}$  is the density of the hybrid nanofluid,  $\mu_{hmf}$  and  $\alpha_{hmf}$  are the dynamic viscosity and thermal diffusivity of the hybrid nanofluid.

Table.2: Thermo-Physical properties comparison between nanofluid and hybrid nanofluid [94]

Properties	Nanofluid	Hybrid nanofluid
Viscosity	$\mu_{nf} = \frac{\mu_f}{(1-\varphi)^{2.5}}$	$\mu_{hnf} = \frac{\mu_f}{(1-\varphi_1)^{2.5}(1-\varphi_2)^{2.5}}$
Density	$\rho_{nf} = \rho_f \left( 1 - \varphi + \varphi \left( \frac{\rho_s}{\rho_f} \right) \right)$	$\rho_{hnf} = \rho_f (1 - \varphi_2) \left( 1 - \varphi_1 + \varphi_1 \left( \frac{\rho_{s1}}{\rho_f} \right) \right) + \varphi_2 \rho_{s2}$
Electric Conductivity	$\sigma_{nf} = \sigma_f \left( 1 + \frac{3 \left( \frac{\sigma_s}{\sigma_f} - 1 \right) \varphi}{2 + \frac{\sigma_s}{\sigma_f} - \left( \frac{\sigma_s}{\sigma_f} - 1 \right) \varphi} \right)$	$\frac{\sigma_{hnf}}{\sigma_f} = 1 + \frac{3\varphi(\varphi_1\sigma_1 + \varphi_2\sigma_2 - \sigma_{bf}\varphi)}{\varphi_1\sigma_1 + \varphi_2\sigma_2 + 2\varphi\sigma_{bf} - \varphi\sigma_{bf}(\varphi_1\sigma_1 + \varphi_2\sigma_2 - \sigma_{bf}\varphi)}$ $\varphi = (\varphi_1 + \varphi_2)$
Coefficient of thermal expansion	$(\rho\beta)_{nf} = (\rho\beta)_f \left( 1 - \varphi + \varphi \frac{(\rho\beta)_s}{(\rho\beta)_f} \right)$	$(\rho\beta)_{hnf} = (\rho\beta)_f (1 - \varphi_2) \left( 1 - \varphi_1 + \varphi_1 \frac{(\rho\beta)_{s1}}{(\rho\beta)_f} \right) + \varphi_2 (\rho\beta)_{s2}$
Heat Capacity	$(\rho Cp)_{nf} = (\rho Cp)_f \left( 1 - \varphi + \varphi \frac{(\rho Cp)_s}{(\rho Cp)_f} \right)$	$(\rho Cp)_{hnf} = (\rho Cp)_f (1 - \varphi_2) \left( 1 - \varphi_1 + \varphi_1 \frac{(\rho Cp)_{s1}}{(\rho Cp)_f} \right) + \varphi_2 (\rho Cp)_{s2}$
Thermal Conductivity	$\frac{k_{nf}}{k_f} = \frac{k_s + (m-1)k_f - (m-1)\varphi(k_f - k_s)}{k_s + (m-1)k_f + \varphi(k_f - k_s)}$	$\frac{k_{hnf}}{k_{bf}} = \frac{k_{s2} + (m-1)k_{bf} - (m-1)\varphi_2(k_{bf} - k_{s2})}{k_{s2} + (m-1)k_{bf} + \varphi_2(k_{bf} - k_{s2})}$ where $\frac{k_{bf}}{k_f} = \frac{k_{s1} + (m-1)k_f - (m-1)\varphi_1(k_f - k_{s1})}{k_{s1} + (m-1)k_f + \varphi_1(k_f - k_{s1})}$

The mass conservation law equation (1) is identically satisfied. However, the radial, tangential and axial momentum equations (replaced with the pressure equation), the energy and the concentration equations are reduced to the equivalent nonlinear coupled system of ordinary differential equations:

$$\frac{f'''}{\varepsilon 1} + \text{Re} \left( 2ff'' - f'^2 + g^2 - \frac{f'}{\varepsilon 3\beta} \right) - \frac{\varepsilon}{\varepsilon 2} - \frac{\varepsilon 4 \text{Re} M f'}{\varepsilon 2} = 0 \quad (9)$$

$$\frac{g''}{\varepsilon 1} + \text{Re} \left( 2fg' - 2f'g - \frac{g}{\varepsilon 3\beta} \right) - \frac{\varepsilon 4 \text{Re} M g}{\varepsilon 2} = 0 \quad (10)$$

$$\frac{P'}{\varepsilon 2} + \frac{2f''}{\varepsilon 1} + 4\text{Re}ff' - \frac{2\text{Re}}{\varepsilon 3\beta}f = 0 \quad (11)$$

$$\frac{1}{\text{PrRe}} \left( \varepsilon 5 + \frac{4}{3} Rd \right) \theta'' + EcM\varepsilon 4(f' + g^2) + (Q\theta + Q_1 \exp^{-\eta}) + 2\varepsilon 6f\theta' = 0 \quad (12)$$

The corresponding boundary conditions (7) at lower and upper disk transform to:

$$\left. \begin{array}{l} \text{Lower disk: } f(0) = -fw, f'(0) = A_1, g(0) = 1, P(0) = 0, \theta'(0) = -B_i(1 - \theta(0)) \\ \text{Upper disk: } f'(1) = A_2, f(1) = 0, g(1) = \tau, \theta(1) = 0 \end{array} \right\} \quad (13)$$

But

$$\varepsilon 1 = (1 - \varphi_1)^{2.5} (1 - \varphi_2)^{2.5} (1 - \varphi_2) \left( 1 - \varphi_1 + \varphi_1 \left( \frac{\rho_{s1}}{\rho_f} \right) \right) + \varphi_2 \rho_{s2}$$

$$\varepsilon 2 = (1 - \varphi_2) \left( 1 - \varphi_1 + \varphi_1 \left( \frac{\rho_{s1}}{\rho_f} \right) \right) + \varphi_2 \rho_{s2}$$

$$\varepsilon 3 = (1 - \varphi_1)^{2.5} (1 - \varphi_2)^{2.5}$$

$$\varepsilon 4 = 1 + \frac{3(\varphi_1 + \varphi_2)(\varphi_1 \sigma_1 + \varphi_2 \sigma_2 - \sigma_{bf}(\varphi_1 + \varphi_2))}{\varphi_1 \sigma_1 + \varphi_2 \sigma_2 + 2(\varphi_1 + \varphi_2) \sigma_{bf} - (\varphi_1 + \varphi_2) \sigma_{bf}(\varphi_1 \sigma_1 + \varphi_2 \sigma_2 - \sigma_{bf}(\varphi_1 + \varphi_2))}$$

$$\varepsilon 5 = \left( \frac{k_{s1} + (m-1)k_f - (m-1)\varphi_1(k_f - k_{s1})}{k_{s1} + (m-1)k_f + \varphi_1(k_f - k_{s1})} \right) \times \left( \frac{k_{s2} + (m-1)k_{bf} - (m-1)\varphi_2(k_{bf} - k_{s2})}{k_{s2} + (m-1)k_{bf} + \varphi_2(k_{bf} - k_{s2})} \right)$$

where

$$k_{bf} = k_f \left( \frac{k_{s1} + (m-1)k_f - (m-1)\varphi_1(k_f - k_{s1})}{k_{s1} + (m-1)k_f + \varphi_1(k_f - k_{s1})} \right)$$

$$\varepsilon 6 = (1 - \varphi_2) \left( 1 - \varphi_1 + \varphi_1 \left( \frac{(\rho Cp)_{s1}}{(\rho Cp)_f} \right) \right) + \varphi_2 (\rho Cp)_{s2}$$

Where  $\beta = \frac{k_0 \Omega_1}{\mu_f}$  denotes the porosity parameter,  $Rd = \frac{4\sigma^* T_2^3}{k^*}$  is the radiative parameter,

$\text{Pr} = \frac{\mu_f Cp_f}{k_f}$  denotes the Prandtl number,  $M = \frac{\sigma_f \beta_0^2}{\rho_f \Omega_1}$  is the magnetic parameter,  $\text{Re} = \frac{\Omega_1 h^2}{\nu_f}$

denotes the Reynolds number,  $Ec = \frac{\Omega_1^2 r^2}{Cp_f (T_1 - T_2)}$  is the Eckert number,  $\tau = \frac{\Omega_2}{\Omega_1}$  denotes the

rotation number  $A_1 = \frac{a_1}{\Omega_1}$  and  $A_2 = \frac{a_2}{\Omega_2}$  are scaled stretching parameters,  $f_w = \frac{W_0}{2h\Omega_1}$  is the

suction/injection parameter,  $B_i = \frac{hh_f}{k_f}$  is the Biot number at the lower disk and upper disk.

For making simpler form of Equation (9) and removing  $\varepsilon$ , it can be differentiated with respect to  $\eta$  and then we have:

$$\frac{f^{iv}}{\varepsilon} + \text{Re} \left( 2ff'' - 2gg' - \frac{f''}{\varepsilon 3\beta} \right) - \frac{\varepsilon 4 \text{Re} M f''}{\varepsilon 2} = 0 \quad (14)$$

#### 4. SKIN FRICTION AND NUSSELT NUMBER

The radial and tangential shear stresses are given as  $\tau_{zr}$ ,  $\tau_{r\theta}$  respectively.

$$\tau_{zr} \text{ at the lower disk is given as } \tau_{zr1} = \mu_{hmf} \left. \frac{\partial u}{\partial z} \right|_{z=0} \Rightarrow \frac{\mu_f r \Omega_1 f''(0)}{(1-\varphi_1)^{2.5} (1-\varphi_2)^{2.5} h} \quad (15)$$

$$\tau_{zr} \text{ at the upper disk is given as } \tau_{zr2} = \mu_{hmf} \left. \frac{\partial u}{\partial z} \right|_{z=h} \Rightarrow \frac{\mu_f r \Omega_1 f''(1)}{(1-\varphi_1)^{2.5} (1-\varphi_2)^{2.5} h} \quad (16)$$

$$\tau_{z\theta} \text{ at the lower disk is given as } \tau_{z\theta 1} = \mu_{hmf} \left. \frac{\partial u}{\partial z} \right|_{z=0} \Rightarrow \frac{\mu_f r \Omega_1 g'(0)}{(1-\varphi_1)^{2.5} (1-\varphi_2)^{2.5} h} \quad (17)$$

$$\tau_{z\theta} \text{ at the upper disk is given as } \tau_{z\theta 2} = \mu_{hmf} \left. \frac{\partial u}{\partial z} \right|_{z=h} \Rightarrow \frac{\mu_f r \Omega_1 g'(1)}{(1-\varphi_1)^{2.5} (1-\varphi_2)^{2.5} h} \quad (18)$$

The total shear stresses at the surface of the lower and upper rotating disks, respectively, are given as:

$$\tau_{w1} = \sqrt{\tau_{zr1}^2 + \tau_{z\theta 1}^2} \quad (19)$$

$$\tau_{w2} = \sqrt{\tau_{zr2}^2 + \tau_{z\theta 2}^2} \quad (20)$$

Therefore the skin friction coefficients  $C_f(0)$  and  $C_f(1)$  at the lower and upper disks, respectively, are as follows:

$$C_f(0) = \frac{\tau_{w1}}{\rho_f (r\Omega_1)^2} = \frac{1}{\text{Re}_r (1-\varphi_1)^{2.5} (1-\varphi_2)^{2.5}} \left[ (f''(0))^2 + (g'(0))^2 \right] \quad (21)$$

$$C_f(1) = \frac{\tau_{w2}}{\rho_f (r\Omega_1)^2} = \frac{1}{\text{Re}_r (1-\varphi_1)^{2.5} (1-\varphi_2)^{2.5}} \left[ (f''(1))^2 + (g'(1))^2 \right] \quad (22)$$

Where  $\text{Re}_r = \frac{r\Omega_1 h}{\nu_f}$  is the local Reynolds number. The Nusselt numbers at the lower and upper disks, respectively, are as follows:

$$Nu_z(0) = \frac{hq_w}{k_f(T_1 - T_2)} \Big|_{z=0} \quad (23)$$

$$Nu_z(1) = \frac{hq_w}{k_f(T_1 - T_2)} \Big|_{z=h} \quad (24)$$

The heat flux  $q_w$  at the lower and upper rotating disks, respectively, are as follows:

$$q_w|_{z=0} = k_{hmf} \frac{\partial T}{\partial z} + q_r|_{z=0} = -\frac{T_1 - T_2}{h} \left( k_{hmf} + \frac{16\sigma^* T_2^3}{3k^*} \right) \theta'(0) \quad (25)$$

$$q_w|_{z=h} = k_{hmf} \frac{\partial T}{\partial z} + q_r|_{z=h} = -\frac{T_1 - T_2}{h} \left( k_{hmf} + \frac{16\sigma^* T_2^3}{3k^*} \right) \theta'(1) \quad (26)$$

hence the Nusselt numbers at the lower and upper rotating disks surfaces, respectively, are written as:

$$Nu_z(0) = -\left( \frac{k_{hmf}}{k_f} + \frac{4}{3} Rd \right) \theta'(0) \quad (27)$$

$$Nu_z(1) = -\left( \frac{k_{hmf}}{k_f} + \frac{4}{3} Rd \right) \theta'(1) \quad (28)$$

## 5. ENTROPY GENERATION AND BEJAN NUMBER

Entropy generation rate is the determination of the irreversibilities encountered in a specific process.

The entropy generation is written as:

$$S_G = \frac{k_{hmf}}{T_f} \left[ \left( \frac{\partial T}{\partial z} \right)^2 + \frac{16\sigma^* T_2^3}{3k^* k_f} \left( \frac{\partial T}{\partial z} \right)^2 \right] + \frac{\mu_{hmf}}{T_f} \Phi + \frac{\sigma_{hmf}}{T_f} \beta_0^2 (u^2 + v^2) \quad (29)$$

where

$$\Phi = 2 \left[ \left( \frac{\partial u}{\partial r} \right)^2 + \frac{1}{r^2} u^2 + \left( \frac{\partial w}{\partial z} \right)^2 \right] + \left( \frac{\partial v}{\partial z} \right)^2 + \left( \frac{\partial w}{\partial r} + \frac{\partial u}{\partial z} \right)^2 + \left[ r \frac{\partial}{\partial r} \left( \frac{v}{r} \right) \right]^2 \quad (30)$$

The entropy generation is the combination of three terms as shown below:

$$S_G = \underbrace{\frac{k_{hmf}}{T_f} \left[ \left( \frac{\partial T}{\partial z} \right)^2 + \frac{16\sigma^* T_2^3}{3k^* k_f} \left( \frac{\partial T}{\partial z} \right)^2 \right]}_{\text{Thermal\_irreversibility}} + \underbrace{\frac{\mu_{hmf}}{T_f} \left[ 2 \left[ \left( \frac{\partial u}{\partial r} \right)^2 + \frac{1}{r^2} u^2 + \left( \frac{\partial w}{\partial z} \right)^2 \right] + \left( \frac{\partial v}{\partial z} \right)^2 + \left( \frac{\partial w}{\partial r} + \frac{\partial u}{\partial z} \right)^2 + \left[ r \frac{\partial}{\partial r} \left( \frac{v}{r} \right) \right]^2 \right]}_{\text{Fluid\_fraction\_irreversibility}} + \underbrace{\frac{\sigma_{hmf}}{T_f} \beta_0^2 (u^2 + v^2)}_{\text{Joule-dissipation-irreversibility}} \quad (31)$$

Substituting the similarity transformation of equation (7) into equation (30), we have:

$$N_G = \frac{k_{hmf}}{k_f} \frac{\alpha_1}{\text{Re}} \left(1 + \frac{4}{3} Rd\right) \theta'^2 + \frac{Br}{\text{Re}} \frac{1}{(1-\varphi_1)^{2.5} (1-\varphi_2)^{2.5}} (Ag'^2 + Af''^2 + 12f'^2) + \varepsilon 4MBrA(f'^2 + g^2) \quad (32)$$

Where

$$N_G = \frac{T_f S_G \nu_f}{k_f (T_1 - T_2) \Omega_1}, Br = \frac{\mu_f r^2 \Omega_1^2}{k_f (T_1 - T_2)}, r^2 = Ah^2, \alpha_1 = \frac{T_1 - T_2}{T_f}$$

Where  $T_f$  denotes the mean temperature,  $N_G$  is the entropy generation rate,  $A$  is the dimensionless radial parameter,  $\alpha_1$  is the dimensionless temperature difference and  $Br$  denotes the Brinkman number.

The Bejan number ( $Be$ ) in a dimensionless form is defined as:

$Be = \text{Entropy generation due to heat transfer} / \text{Total entropy generation.}$

$$Be = \frac{\frac{k_{hmf}}{k_f} \frac{\alpha_1}{\text{Re}} \left(1 + \frac{4}{3} Rd\right) \theta'^2}{\frac{k_{hmf}}{k_f} \frac{\alpha_1}{\text{Re}} \left(1 + \frac{4}{3} Rd\right) \theta'^2 + \frac{Br}{\text{Re}} \frac{1}{(1-\varphi_1)^{2.5} (1-\varphi_2)^{2.5}} (Ag'^2 + Af''^2 + 12f'^2) + \varepsilon 4MBrA(f'^2 + g^2)} \quad (33)$$

## 6. NUMERICAL SOLUTION

Equations (10), (11), (12) and (14) along with the associated boundary conditions (13) were solved numerically via Newton's finite difference method with the help of Maple 18.0 software. In this method, the system of ODEs is converted to a first-order system by introducing a new dependent variable then the derivatives are replaced by finite-difference approximations, to form a system of algebraic equations; a mesh of evenly spaced points is then defined on the solution interval and the algebraic equations are solved at the mesh points by Newton's iteration scheme.

The solution depend on porosity parameter ( $\beta$ ), radiative parameter parameter ( $Rd$ ), magnetic parameter ( $M$ ), Reynolds number ( $Re$ ), relative rotational parameter ( $\tau$ ), suction/injection

parameter ( $f_w$ ), Prandtl number ( $Pr$ ) and upper and lower scaled stretching parameter ( $A_1$ ) and ( $A_2$ ) respectively. The effects of parameters were discussed and graphical results were presented to explore stimulating aspects of the parameters on related profiles.

## 7. RESULTS AND DISCUSSION

In this paper, the theoretical analysis of hybrid nanofluid flow due to stretchable rotating disks system under the influence of non-uniform heat source or sink and thermal radiation. Two types of nanoparticles Copper (Cu) and Alumina ( $Al_2O_3$ ) mixed with the base fluid (ethylene glycol and water) in a ratio 50:50 were considered, the effect of flow parameters were obtained from the solution. The purpose of this section is to interpret the graphical description of sundry variables such as local Reynolds number ( $Re$ ), Magnetic parameter ( $M$ ), Stretching rate parameter at the lower disk ( $A_1$ ), Stretching rate parameter at the upper disk ( $A_2$ ) on axial velocity  $f(\eta)$ , radial velocity  $f'(\eta)$ , tangential velocity  $g(\eta)$  and the thermal field  $\theta(\eta)$ . Figure.2a, b and d, shows a direct relationship between the Reynolds number ( $Re$ ) and the axial, radial and the temperature profiles respectively, which implies that profiles are increasing as we increase ( $Re$ ) while Figure.2c indicate otherwise, as the Reynolds number ( $Re$ ) increases the tangential velocity decreases.

The effect of the stretching parameter at the lower disk ( $A_1$ ) is observed in Figure.3. As shown in Figure.3a and b, the axial and the radial velocities increase respectively with increment in the stretching rate parameter at the lower disk. In Figure.3c and d, the tangential and the temperature profiles decays respectively near the lower disc with increasing ( $A_1$ ).

Figure.4 analyzed the impact of stretching rate parameter at the upper disk ( $A_2$ ). Here in Figure.4a and b, the axial and radial velocities decays respectively for higher stretching rate parameter at the upper disk ( $A_2$ ) while Figure.4c and d are directly promotional to the tangential and temperature profiles respectively with increasing ( $A_2$ ).

Characteristics of skin friction coefficient at the lower and upper disk versus Reynolds number for different magnetic parameter ( $M$ ) are shown on Figure.5 and 6 respectively. The skin friction coefficients are increasing on both graphs.

Figure.7 and 8 displayed the behaviour of Nusselt number at the lower and upper disks respectively versus the Reynolds number for different magnetic parameter ( $M$ ). It is noted that the Nusselt number at the lower and upper disks increases for larger magnetic parameter.

The total entropy generation and Bejan number at the lower disk were discussed in Figure.9 and 10 respectively with increasing Reynolds number, the entropy generation decreases which is obvious as shown in equation (32) where the non-dimensional entropy generation is

inversely proportional to the Reynolds number (see Figure.9). Also the Bejan number reduces with increasing Reynolds number (see Figure.10).The effect of (Q) and (Q<sub>1</sub>) are demonstrated on Fig.11 and Fig.12 respectively. It was found that both (Q) and (Q<sub>1</sub>) enhance the thermal field. Fig.13, it was found that an increase in radiation parameter (Rd) enhance the absorbing rate (k\*) which decrease the temperature profile. Fig.14 shows the impact of increasing magnetic field parameter (M) on the thermal field; (M) is noticeably increasing.

The comparison results of skin friction coefficient and Nusselt number of some existing literature: Turkyilmazoglu *et al* [28], Hosseinzadeh *et al* [29] and Sachin Shaw [94], under some certain conditions (absent of hybrid nanoparticles: φ<sub>1</sub>=φ<sub>2</sub>=0) were tabulated on Table.3and 4 respectively. Table.5 illustrated the behaviour of skin friction coefficient at the lower and upper rotating disk for different parameters. Table.6 illustrated the behaviour of Nusselt number at the lower and upper rotating disk for different parameters. The impact of the total entropy generation and Bejan number are tabulated for different parameters on Table.7.

Table.3: Comparison table for values of Ω obtained for φ<sub>1</sub>=φ<sub>2</sub>=Q=Q<sub>1</sub>=Rd=M=β=A<sub>1</sub>=A<sub>2</sub>=Ec=0,Re=1.

Ω	<i>f</i> ''(0)[28]	<i>f</i> ''(0)[29]	<i>f</i> ''(0)[94]	Present work
-1	0.06666313	0.06666265832	0.06666265672	0.06666265784
-0.8	0.08394206	0.08394497836	0.08394497811	0.08394497789
-0.3	0.10395088	0.1039497753	0.10394977482	0.10394977522
0.0	0.09997221	0.09996773288	0.09996773274	0.09996773292
0.5	0.06663419	0.06663026596	0.06663026575	0.06663026584

Table.4: Comparison table for values of Ω obtained for φ<sub>1</sub>=φ<sub>2</sub>=Q=Q<sub>1</sub>=Rd=M=β=A<sub>1</sub>=A<sub>2</sub>=Ec=0,Re=1.

Ω	<i>g</i> '(0)[28]	<i>g</i> '(0)[29]	<i>g</i> '(0)[94]	Present work
-1	2.00095215	2.000952381	2.000952292	2.000952354
-0.8	1.80258847	1.802594286	1.802594279	1.802594280
-0.3	1.30442355	1.304432381	1.304432380	1.304432378
0.0	1.00427756	1.004285714	1.004285716	1.004285715
0.5	0.50261351	0.5026190476	0.5026190474	0.502619047

Table. 5: Skin friction at the lower and upper rotating disk for different parameters.

M	Re	$\beta$	$f_w$	A <sub>1</sub>	A <sub>2</sub>	$C_f(0)$	$C_f(1)$
2.0	0.5	0.3	0.1	0.1	0.1	1.05144660624814	0.484521102565349
3.0	-	-	-	-	-	1.23956828020886	0.601753627545389
5.0	-	-	-	-	-	1.63266124217681	0.853133149461925
2.0	0.8	-	-	-	-	1.95597199236880	1.08468123597066
3.0	-	-	-	-	-	2.28622764371762	1.30584789533607
5.0	-	-	-	-	-	2.96143775945779	1.76207691672611
2.0	1.0	-	-	-	-	2.58685632450663	1.52642271002067
3.0	-	-	-	-	-	3.00837338466685	1.81436673224480
5.0	-	-	-	-	-	3.86243877374415	2.39942140749220

Table. 6: Nusselt number at the lower and upper rotating disk for different parameters.

M	Re	Pr	Rd	Q	Q <sub>1</sub>	B <sub>i</sub>	Ec	$Nu_z(0)$	$Nu_z(1)$
2.0	0.5	0.07	0.1	0.1	0.1	0.1	0.5	0.0619155174437872	0.107906632229096
3.0	-	-	-	-	-	-	-	0.0622197791140176	0.122960200413254
5.0	-	-	-	-	-	-	-	0.0628274395530562	0.151360203157554
2.0	0.8	-	-	-	-	-	-	0.0624364207014617	0.135875572225952
3.0	-	-	-	-	-	-	-	0.0629229300321823	0.158775531153162
5.0	-	-	-	-	-	-	-	0.0638940947191340	0.201395194301473
2.0	1.0	-	-	-	-	-	-	0.0627843738415703	0.155256286907528
3.0	-	-	-	-	-	-	-	0.0633924053193499	0.183365803518309
5.0	-	-	-	-	-	-	-	0.0646058250213665	0.235409348881533

Table. 7: Entropy generation and Bejan number at the lower rotating disk for different parameters.

M	Re	Pr	Rd	A	$\alpha_1$	Br	$N_G(0)$	$B_e(0)$
2.0	0.5	0.07	0.1	0.1	0.1	0.3	0.211534850521512	0.0582865177515803
3.0	-	-	-	-	-	-	0.242231882518738	0.0509001114626034
5.0	-	-	-	-	-	-	0.304228943431984	0.0405274714526185
2.0	0.8	-	-	-	-	-	0.186317957308928	0.0413595058109341
3.0	-	-	-	-	-	-	0.217621756829765	0.0354101480948343
5.0	-	-	-	-	-	-	0.280641737469940	0.0274585623203156
2.0	1.0	-	-	-	-	-	0.178279597518223	0.0345794751436426
3.0	-	-	-	-	-	-	0.209750697600864	0.0293911533144508
5.0	-	-	-	-	-	-	0.273009321131411	0.0225809686110777

$$\beta=0.9, \tau=0.8, A_2=0.4, M=2.0, Ec=0.5, A_1=Rd=Q=Q_1=B_i=fw=\phi_1=\phi_2=0.1$$

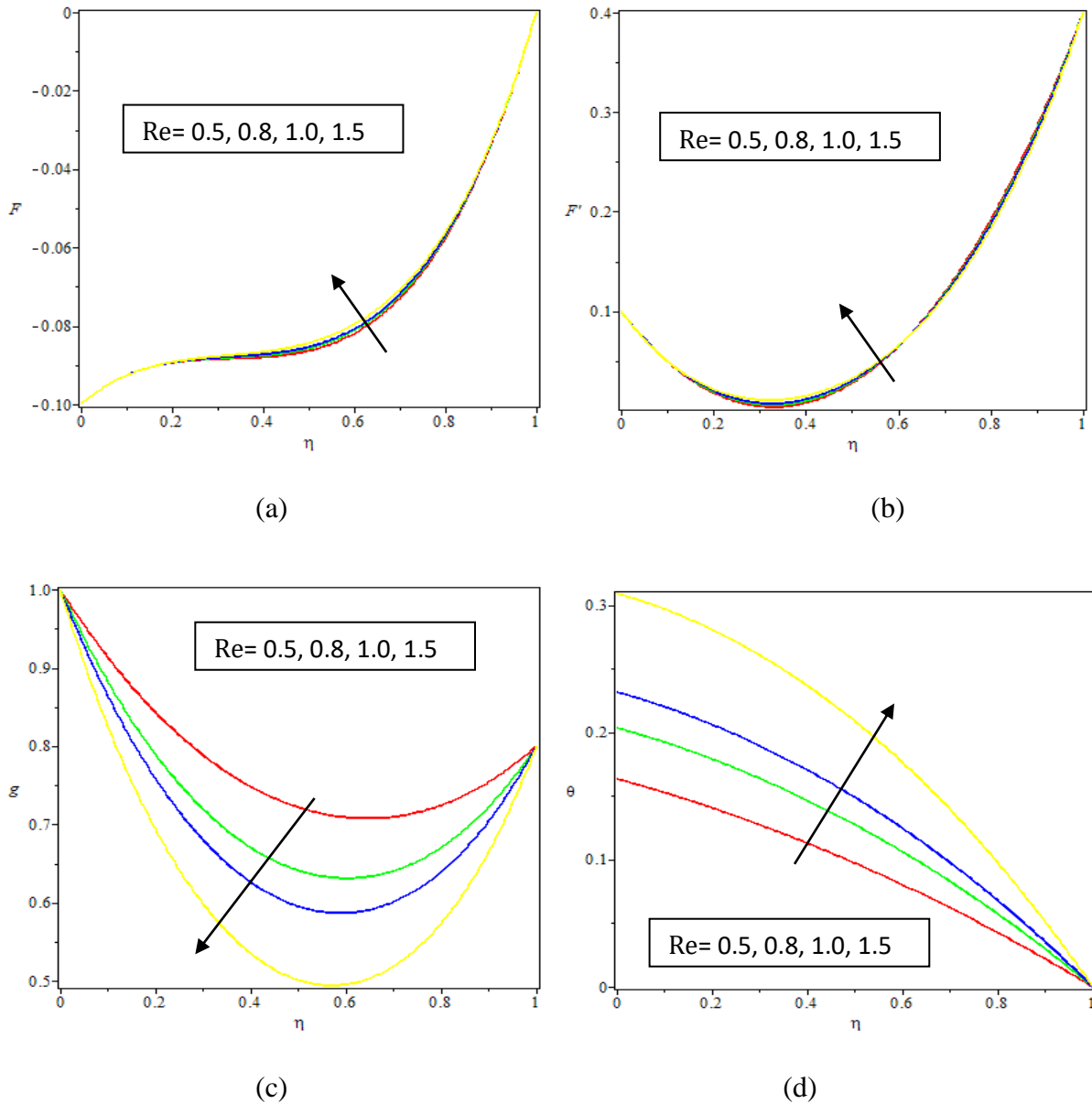


Figure.2. Effect of Reynolds number (Re) on axial velocity (f), Radial velocity (f'), tangential velocity (g) and Temperature profile ( $\theta$ )

$$\beta=0.9, \tau=0.8, A_2=0.4, M=2.0, Ec=0.5, Re=1.0, Rd=Q=Q_1=B_1=fw=\varphi_1=\varphi_2=0.1$$

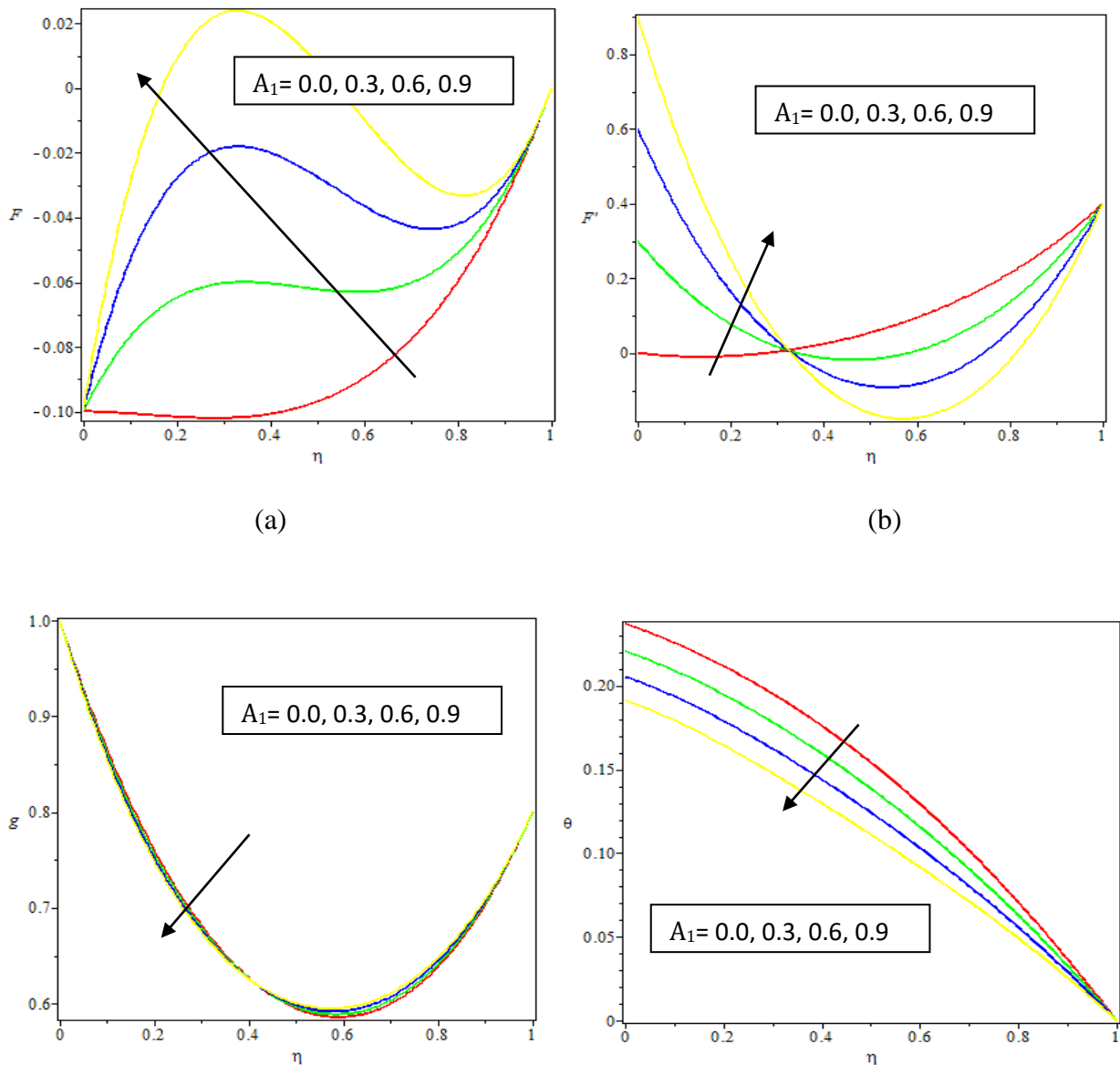


Figure.3. Effect of Stretching parameter at the lower disc ( $A_1$ ) on axial velocity ( $f$ ), Radial velocity ( $f'$ ), tangential velocity ( $g$ ) and Temperature profile ( $\theta$ )

$$\beta=0.9, \tau=0.8, A_1=0.2, M=2.0, Ec=0.5, Re=1.0, Rd=Q=Q_1=B_1=fw=\varphi_1=\varphi_2=0.1$$

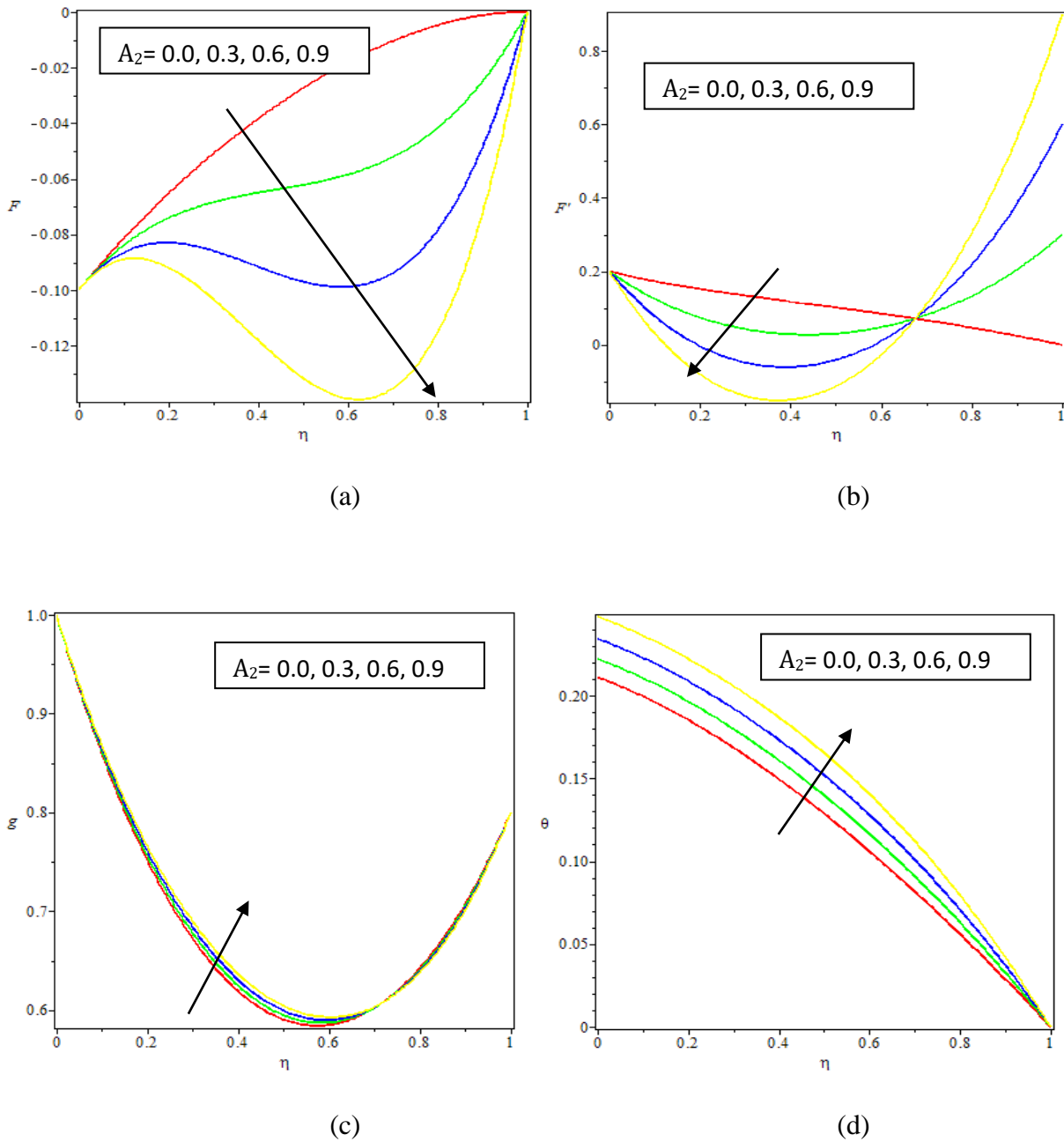


Figure.4. Effect of Stretching parameter at the upper disc ( $A_2$ ) on axial velocity ( $f$ ), Radial velocity ( $f'$ ), tangential velocity ( $g$ ) and Temperature profile ( $\theta$ )

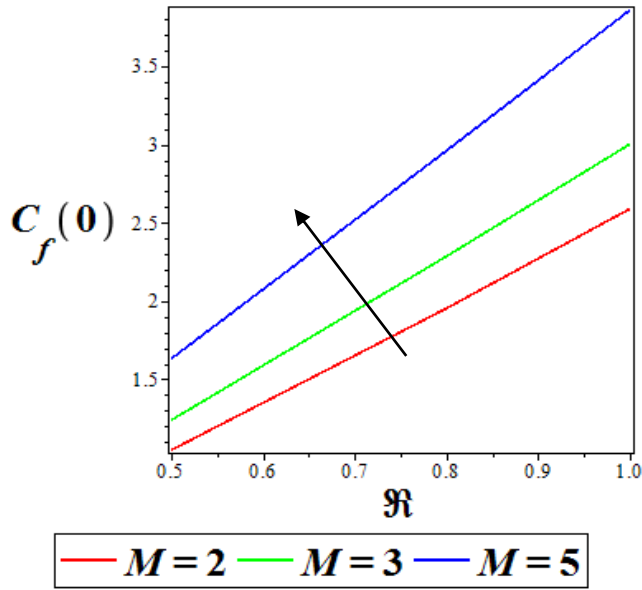


Figure.5. Effect of the Skin friction at the lower disk Vs. Re for different M

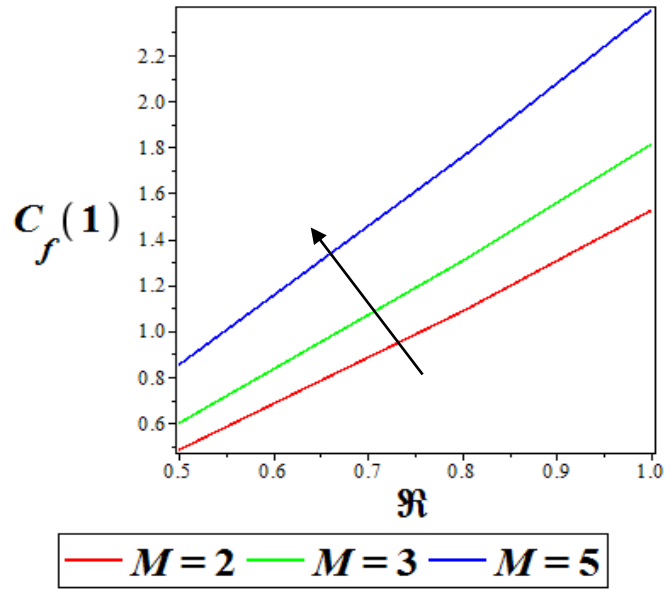


Figure.6. Effect of the Skin friction at the upper disk Vs. Re for different M

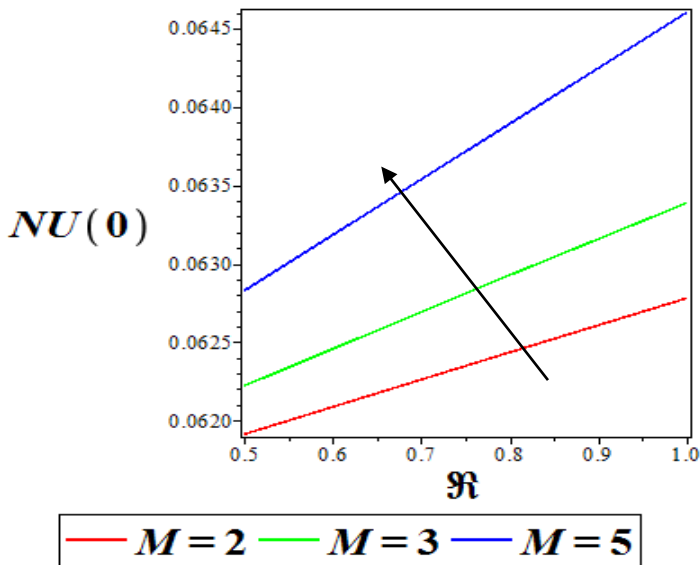


Figure.7. Effect of the Nusselt number at the lower disk Vs. Re for different M

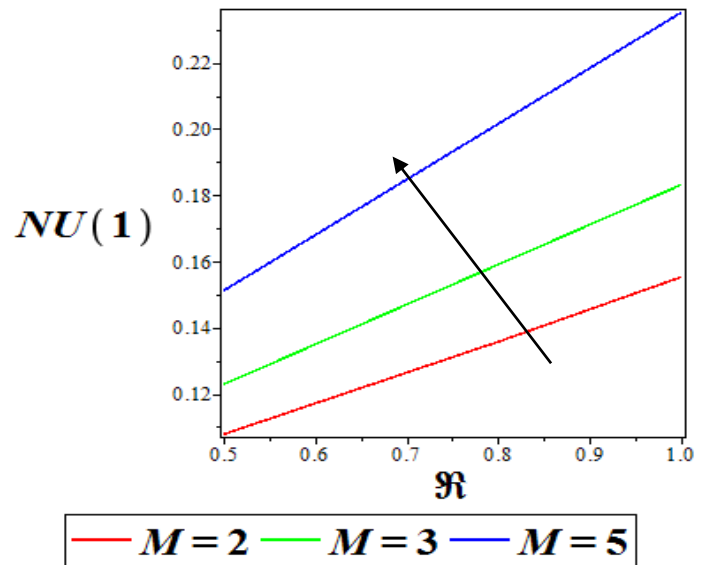


Figure.8. Effect of the Nusselt number at the upper disk Vs. Re for different M

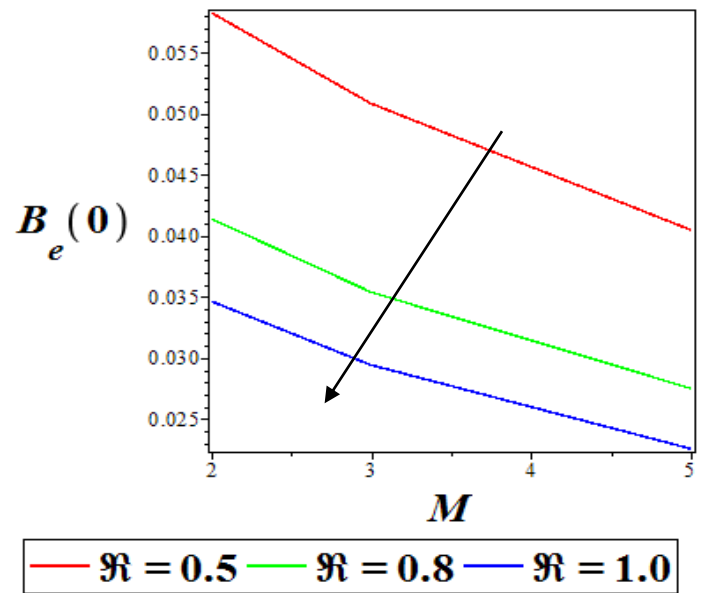
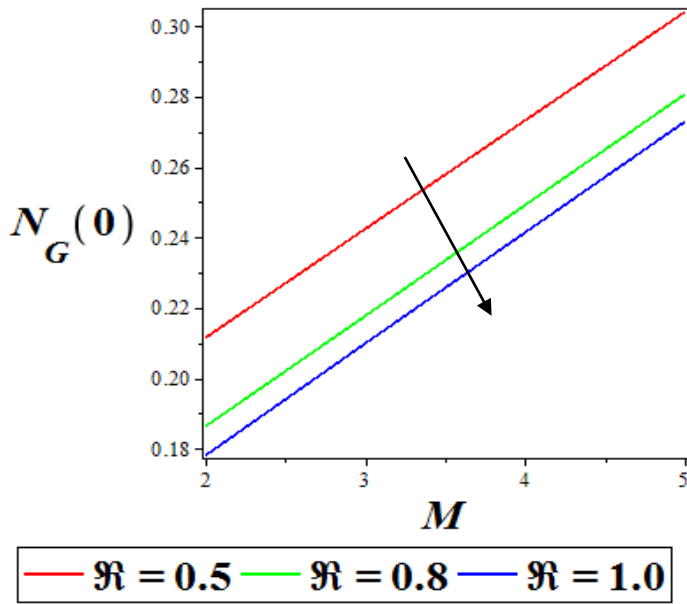


Figure.9. Entropy generation at the lower disk Vs M for various Re

Figure.10. Bejannumber at the lower disk Vs M for various Re

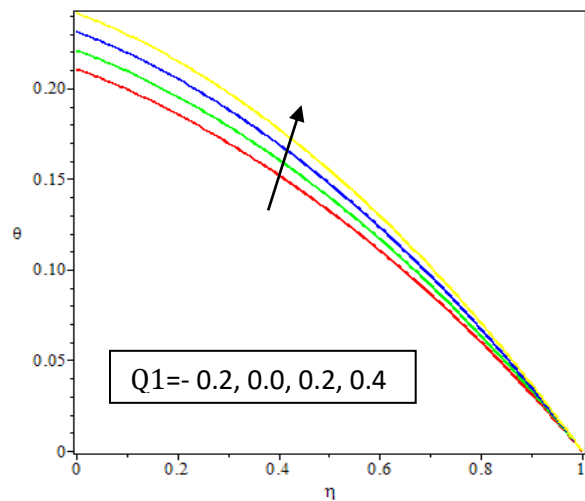
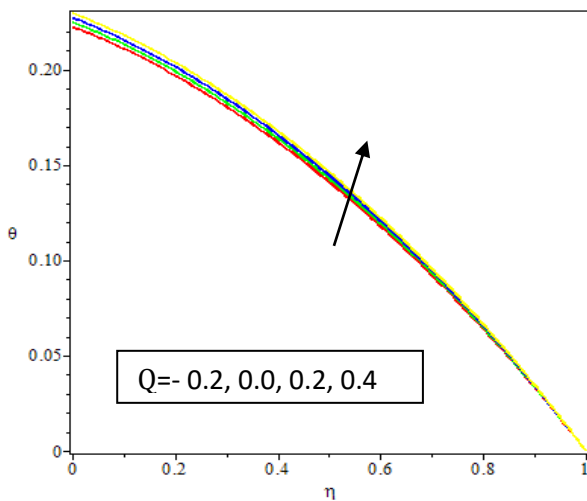


Figure.11. Effect of Q on Temperature profile ( $\theta$ )

Figure.12. Effect of Q1 on Temperature profile ( $\theta$ )

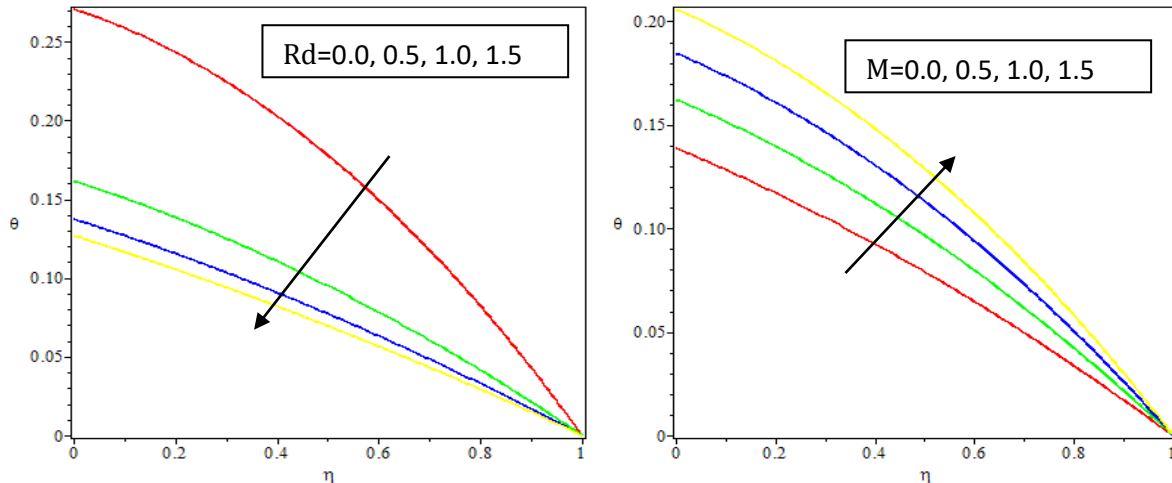


Figure.13. Effect of  $Rd$  on Temperature profile ( $\theta$ ) Figure.14. Effect of  $M$  on Temperature profile ( $\theta$ )

## 8. CONCLUSION

In this paper, the effect of Reynolds number, stretching rate parameter at the lower and upper disk, skin friction coefficient at the lower and upper disk, Nusselt number at the lower and upper disk, the total entropy generation, Bejan number, radiation parameter, temperature dependent heat source parameter, surface dependent heat source parameter and magnetic parameter on the Mixture of  $\text{Al}_2\text{O}_3\text{-Cu}/\text{H}_2\text{O}-(\text{CH}_2\text{OH})_2$  MHD hybrid nanofluid flow due to a stretchable rotating disks system have been investigated using the Newton's finite differential method. It is confirmed in this work that the radiation parameter enhance the adsorption rate which decreases the temperature profile. Base on the work the following remarks were made.

- 1) As the Reynolds number increase, the axial, radial and thermal field increases significantly while tangential velocities decrease.
- 2) Increasing the stretching rate parameter at the lower disk ( $A_1$ ), the axial and the radial velocities enhances near the lower disk while the tangential velocity and the temperature profile decreases near the lower disk but the impact of increasing stretching rate parameter at the upper disk ( $A_2$ ) is the opposite of ( $A_1$ ) on all the profiles.
- 3) Increasing the temperature dependent heat source parameter and the surface dependent heat source parameter evokes a corresponding increase in the thermal field for both parameters.
- 4) By increasing the Reynolds number, the total entropy generation and Bejan number at the lower disk decreases, which are obvious as shown in equation (32) where the non-dimensional entropy generation is inversely proportional to the Reynolds number.

## CONFLICT OF INTERESTS

The author(s) declare that there is no conflict of interests.

**REFERENCES**

- [1] F. Mirzajani, H. Askari, S. Hamzelou, M. Farzaneh, A. Ghassempour, Effect of silver nanoparticles on *Oryzasativa* L. and its rhizo sphere bacteria, *Ecotoxicol. Environ. Saf.* 88 (2013), 48-54.
- [2] T. Von Kármán, Uber laminare and turbulent, *Math. Mech.* 1 (1921), 23-52.
- [3] Tasawar Hayat, Madiha Rashid, Maria Imtiaz, Ahmed Alsaedi, Magnetohydrodynamic (MHD) flow of Cu-water nanofluid due to a rotating disk with partial slip, *AIP Adv.* 5 (2015), 067169.
- [4] M.R. Zangoee, Kh. Hosseinzadeh, D.D. Ganji, Hydrothermal analysis of MHD nanofluid (TiO<sub>2</sub>-GO) flow between two radiative stretchable rotating disks using AGM, *Case Stud. Therm. Eng.* 14 (2019), 100460.
- [5] Chaoli Zhang, Liancun Zheng, Xinxin Zhang, Goong Chen, MHD flow and radiation heat transfer of nanofluids in porous media with variable surface heat flux and chemical reaction, *Appl. Math. Model.* 39 (2015), 165–181.
- [6] Mustafa Turkyilmazoglu, Nanofluid flow and heat transfer due to a rotating disk, *Computers Fluids* 94 (2014), 139–146.
- [7] A. Mushtaq, M. Mustafa, Computations for nanofluid flow near a stretchable rotating disk with axial magnetic field and convective conditions, *Result Phys.* 7 (2017), 3137-3144.
- [8] A. O. Akindele, Amos Wale Ogunsola, A study of non-isothermal permeable flow of nano-fluid in a stretchable rotating disk system, *J. Math. Comput. Sci.* 11 (2021), 1486-1498.
- [9] V. K. Joshi, D. Tripathi, P. Ram, K. Sharma, Numerical investigation of magnetic nanofluids flow over rotating disk embedded in a porous medium. *Research Gate* (2017).
- [10] M. Turkyilmazoglu, MHD fluid flow and heat transfer due to a stretching rotating disk, *Int. J. Therm. Sci.* 51 (2012), 195-201.
- [11] C. Yin, L. Zheng, C. Zhang, X. Zhang, Flow and heat transfer of nanofluids over a rotating disk with uniform stretching rate in the radial direction, *Propuls. Power Res.* 6 (2017), 25-30.
- [12] T. Hayat, M. Rashid, M. Imtiaz, A. Alsaedi, Nanofluid flow due to rotating disk with variable thickness and homogeneous-heterogeneous reactions, *Int. J. Heat Mass Transfer*, 113 (2017), 96-105.
- [13] A. Aziz, A. Alsaedi, T. Muhammad, T. Hayat, Numerical study for heat generation/absorption in flow of nanofluid by a rotating disk, *Results Phys.* 8 (2018), 785-792.
- [14] M. Sheikholeslami, M. Hatami, D. D. Ganki, Numerical investigation of nanofluids flowing on an inclined rotating disk for cooling process, *J. Mol. Liquids*, 211 (2015), 577-583.
- [15] M. Khan, W. Ali, J. Ahmed, A hybrid approach to study the influence of Hall current in radiative nanofluid flow over a rotating disk, *Appl. Nanosci.* 10 (2020), 5167–5177.
- [16] A. J. Chamkha, A. S. Dogonchi, D. D. Ganji, Magneto-hydrodynamic flow and heat transfer of a hybrid nanofluid in a rotating system among two surfaces in the presence of thermal radiation and Joule heating, *AIP Adv.* 9 (2019), 025103.
- [17] A. O. Akindele, O. A. Ajala, P. Adegbite, A. W. Ogunsola, Convective Flow of Nanofluids Using Blasius-Rayleigh-Stoke Variable with Slip Effect, *IOSR J. Math.* 17 (2021), 01-08.
- [18] Z. Shah, A. Dawar, P. Kumam, W. Khan, S. Islam, Impact of Nonlinear Thermal Radiation on MHD Nanofluid Thin Film Flow over a Horizontally Rotating Disk, *Appl. Sci.* 9 (2019), 1533.

- [19] M. Imtiaz, T. Hayat, A. Alsaedi, B. Ahmad, Convective flow of carbon nanotubes between rotating stretchable disks with thermal radiation effects, *Int. J. Heat Mass Transfer*, 101 (2016), 948-957.
- [20] M. Abdel-Wahed, M. Akl, Effect of hall current on MHD flow of a nanofluid with variable properties due to a rotating disk with viscous dissipation and nonlinear thermal radiation, *AIP Adv.* 6 (2016), 095308.
- [21] A. O. Akindele, A. W. Ogunsola, A. M. Obalalu, P. Adegbite, O. A. Ajala, S. Alao, Mhd flow of nano-fluid with non-uniform heat source or sink in the presence of chemical reaction and activation energy, *J. Adv. Res. Appl. Sci.* 7 (2021), 01-15.
- [22] S. P. Anjali Devi, R. Uma Devi, Soret and Dufour effects on MHD slip flow with thermal radiation over a porous rotating infinite disk, *Commun. Nonlinear Sci. Numer. Simul.* 16 (2011), 1917-1930.
- [23] S. Nadeem, M. Ijaz, M. Ayub, Darcy–Forchheimerflow under rotating disk and entropy generation, *J. Therm. Anal. Calorimetry* (2020).
- [24] O. A. Martins, K. Issa, A. Abdulraheem, et al. Numerical simulation of entropy generation for casson fluid flow through permeable walls and convective heating with thermal radiation effect, *J. Serbian Soc. Comput. Mech.* 14 (2020), 149-165.
- [25] O. A. Ajala, A. M. Obalalu, S. F. Abimbade, O. T. Akinyemi, Numerical study of forced convective heat generation flow through a permeable walls with suction/injection, *Int. J. Sci. Res. Publ.* 9 (2019), 336-348.
- [26] A. Bejan, Second-law analysis in heat transfer and thermal design, *Adv. Heat Transfer.* 15 (1982), 1-58.
- [27] A.W. Ogunsola, P.O. Olanrewaju, F.I. Alao, R. Osinowo, O. J. Fenuga, effects of thermal diffusion and diffusion thermo on mhd combined convection and mass transfer past a vertical porous plate embedded in a porous medium with heat generation, thermal radiation, nth order chemical reaction and viscous dissipation, *J. Sci. Eng. Res.* 1 (2014), 1-19.
- [28] M. Turkyilmazoglu, Flow and Heat Simultaneously Induced by Two Stretchable Rotating Disks, *Phys. Fluid*, 28 (2016), 043601.
- [29] K. Hosseinzadeh, A. R. Mogharrebi, A. Asadi, M. Sheikhshahrokhdehordi, S. Mousavisani, D. D. Ganji, Entropy generation analysis of mixture nanofluid ( $\text{H}_2\text{O/C}_2\text{H}_6\text{O}_2$ ) –  $\text{Fe}_3\text{O}_4$  flow between two stretching rotating disks under the effect of MHD and nonlinear thermal rotation, *Int. J. Amb. Energy* (2019).  
<https://doi.org/10.1080/01430750.2019.1681294>
- [30] F. Mabood, T. A. Yusuf, W. A. Khan,  $\text{Cu-Al}_2\text{O}_3\text{-H}_2\text{O}$  hybrid nanofluid flow with melting heat transfer, irreversibility analysis and nonlinear thermal radiation, *J. Therm. Anal. Calorimetry* (2020).
- [31] F. R. Siddiqui, C. Y. Tso, K. C. Chan, S. C. Fu, C. Chao, On trade-off for dispersion stability and thermal transport of  $\text{Cu-Al}_2\text{O}_3$  hybrid nanofluid for various mixing ratios, *Int. J. Heat Mass Transfer*, 132 (2019), 1200-1216.
- [32] S. S. Ghadikolaei, M. Yassari, H. Sadeghi, K. Hosseinzadeh, D. D. Ganji, Investigation on thermophysical properties of  $\text{TiO}_2\text{-Cu/H}_2\text{O}$  hybrid nanofluid transport dependent on shape factor in MHD stagnation point flow, *Powder Technol.* 322 (2020), 428-438.
- [33] B. J. Giresha, G. Sowmya, M. I. Khan, H. F. Oztop, Flow of hybrid nanofluid across a permeable longitudinal moving fin along with thermal radiation and natural convection, *Computer Meth. Programs Biomed.* 185 (2020), 105166.

- [34] I. Waini, A. Ishak, I. Pop, MHD flow and heat transfer of a hybrid nanofluid past a permeable stretching/shrinking wedge, *Appl. Math. Mech.* 41 (2020), 507-520.
- [35] S. A. Khan, M. I. Khan, T. Hayat, A. Alsaedi, Darcy-Forchheimer hybrid (MoS<sub>2</sub>, SiO<sub>2</sub>) nanofluid flow with entropy generation, *Computer Meth. Programs Biomed.* 185 (2020), 105152.
- [36] R. Ellahi, F. Hussain, S. A. Abbas, M. M. Sarafraz, M. Goodarzi, M. S. Shadloo, Study of Two-Phase Newtonian Nanofluid Flow Hybrid with Hafnium Particles under the Effects of slip, *Inventions*, 5 (2020), 6.
- [37] I. Waini, A. Ishak, I. Pop, Hybrid nanofluid flow past a permeable moving thin needle, *Mathematics*, 8 (2020), 612.
- [38] N. Aladdin, N. Bachok, I. Pop, Cu-Al<sub>2</sub>O<sub>3</sub>/water hybrid nanofluid flow over a permeable moving surface in presence of hydromagnetic and suction effects, *Alexandria Eng. J.* 59 (2020), 657-666.
- [39] T. Tayebi, A. J. Chamkha, Natural convection enhancement in an eccentric horizontal cylindrical annulus using hybrid nanofluids, *Numer. Heat Transfer, Part A*, 71 (2017), 1159-1173.
- [40] T. Tayebi, A. J. Chamkha, Free convection enhancement in an annulus between horizontal confocal elliptical cylinders using hybrid nanofluids, *Numer. Heat Transfer, Part A*, 70 (2016), 1141-1156.
- [41] R. Gorla, S. Siddiqua, M. A. Mansour, A. M. Rashad, T. Salah, Heat source/sink effects on a hybrid nanofluid-filled porous cavity, *J. Thermophys. Heat Transfer*, 31 (2017), 847-857.
- [42] A. J. Chamkha, I. V. Miroschnichenko, M. A. Sheremet, Numerical analysis of unsteady conjugate natural convection of hybrid water-based nanofluid in a semi circular cavity, *J. Therm. Sci. Eng. Appl.* 9 (2017), 041004.
- [43] U. Farooq, M. I. Afridi, M. Qasim, D. C. Lu, Transpiration and Viscous Dissipation Effects on Entropy Generation in Hybrid Nanofluid Flow over a Nonlinear Radially Stretching Disk, *Entropy*, 20 (2018), 668.
- [44] M. I. Afridi, T. A. Alkanhal, M. Qasim, I. Tlili, Entropy Generation in Cu-Al<sub>2</sub>O<sub>3</sub>- H<sub>2</sub>O Hybrid Nanofluid Flow over a Curved Surface with Thermal Dissipation, *Entropy*, 21 (2019), 941.
- [45] I. M. Khan, A. Alsaedi, S. Ahmad, T. Hayat, Computational analysis of nanofluid and hybrid nanofluid in Darcy's squeezing flow with entropy optimization, *Int. J. Numer. Meth. Heat Fluid Flow*, 29 (2019), 3394-3416.
- [46] M. I. Khan, M. U. Hafeez, T. Hayat, M. I. Khan, A. Alsaedi, Magneto rotating flow of hybrid nanofluid with entropy generation, *Computer Meth. Programs Biomed.* 183 (2020), 105093.
- [47] H. Sadaf, S. I. Abdelsalam, Adverse effects of a hybrid nanofluid in a wavy non-uniform annulus with convective boundary conditions, *RSC Adv.* 10 (2020), 15035-15043.
- [48] K. Mahammad, T. Hayat, A. Alsaedi, B. Ahmad, S. Momani, Mixed convective slip flow of hybrid nanofluid (MWCNTs + Cu + Water), nanofluid (MWCNTs + Water) and base fluid (Water): a comparative investigation, *J. Therm. Anal. Calorimetry* (2020).
- [49] N. A. Zainala, R. Nazar, K. Naganthran, I. Pop, MHD mixed convection stagnation point flow of a hybrid nanofluid past a vertical flat plate with convective boundary condition, *Chinese J. Phys.* 66 (2020), 630-644.
- [50] B. Venkateswarlu, P. Narayana, Cu<sub>2</sub>Al<sub>2</sub>O<sub>3</sub>/H<sub>2</sub>O hybrid nanofluid flow past a porous stretching sheet due to temperature dependent viscosity and viscous dissipation, *Heat Transfer* (2020).

- [51] N. C. Roy, L. K. Saha, M. Sheikholeslami, Heat transfer of a hybrid nanofluid past acircular cylinder in the presence of thermal radiation and viscous dissipation, *AIP Adv.* 10, (2020), 095208.
- [52] A. Ali, A. Noreen, S. Saleem, A. F. Aljohani, M. Awais, Heat transfer analysis of Cu– $\text{Al}_2\text{O}_3$  hybrid nanofluid with heat flux and viscous dissipation, *J. Therm. Anal. Calorim.* (2020).
- [53] E. H. Aly, I. Pop, MHD flow and heat transfer near stagnation point over a stretching/shrinking surface with partial slip and viscous dissipation: Hybrid nanofluid versus nanofluid, *Powder Technol.* 367 (2020), 192-205.
- [54] N. Acharya, S. Maity, P. K. Kundu, Framing the hydrothermal features of magnetized  $\text{TiO}_2\text{-CoFe}_2\text{O}_4$  water-based steady hybrid nanofluid flow over a radiative revolving disk, *Multidiscip. Model. Mater. Struct.* 16 (2019), 765-790.
- [55] M. Usman, M. Hamid, T. Zubair, R. U. Haq, W. Wang, Cu- $\text{Al}_2\text{O}_3$ /Water hybrid nanofluid through a permeable surface in the presence of nonlinear radiation and variable thermal conductivity via LSM, *Int. J. Heat Mass Transfer*, 126 (2018), 1347-1356.
- [56] B. J. Gireesha, G. Sowmya, M. I. Khan, H. F. Öztop, Flow of hybrid nanofluid across a permeable longitudinal moving fin along with thermal radiation and natural convection, *Computer Meth. Programs Biomed.* 185, (2020), 105166.
- [57] M. Ghalambaz, M. Sabour, I. Pop, D. Wen, Free convection heat transfer of MgO- MWCNTs/EG hybrid nanofluid in a porous complex shaped cavity with MHD and thermal radiation effects, *Int. J. Numer. Meth. Heat Fluid Flow*, 29 (2019), 4349-4376.
- [58] N. S. Khashi'ie, N. M. Arifin, I. Pop, R. Nazar, E. H. Hafidzuddin, N. Wahi, Three-Dimensional Hybrid Nanofluid Flow and Heat Transfer past a Permeable Stretching/Shrinking Sheet with Velocity Slip and Convective Condition, *Chinese J. Phys.* 66 (2020), 157-171.
- [59] M. Izadi, M. A. Sheremet, S. Mehryan, Natural convection of a hybrid nanofluid affected by an inclined periodic magnetic field within a porous medium, *Chinese J. Phys.* 65 (2020), 447-458.
- [60] N. S. Khashi'ie, N. M. Arifin, I. Pop, N. S. Wahid, Flow and heat transfer of hybrid nanofluid over a permeable shrinking cylinder with Joule heating: A comparative analysis, *Alexandria Eng. J.* 59 (2020), 1787-1798.
- [61] S. S. Ghadikolaei, M. Gholinia, 3D mixed convection MHD flow of GO-MoS<sub>2</sub> hybrid nanoparticles in  $\text{H}_2\text{O-(CH}_2\text{OH)}_2$  hybrid base fluid under the effect of H<sub>2</sub> bond, *Int. Commun. Heat Mass Transfer*, 110 (2020), 104371.
- [62] C. Ouyang, R. Akhtar, M. Raja, M. T. Sabir, M. Awais, M. Shoaib, Numerical treatment with Lobatto IIIA technique for radiative flow of MHD hybrid nanofluid ( $\text{Al}_2\text{O}_3\text{-Cu/H}_2\text{O}$ ) over a convectively heated stretchable rotating disk with velocity slip effects, *AIP Adv.* 10 (2020), 055122.
- [63] N. Acharya, R. Bag, P. K. Kundu, Influence of Hall current on radiative nanofluid flow over a spinning disk: A hybrid approach, *Physica E: Low-dimensional Syst. Nanostruct.* 111 (2019), 103-112.
- [64] H. Xu, Modeling unsteady mixed convection of a nanofluid suspended with multiple kinds of nanoparticles between two rotating disks by generalized hybrid model, *Int. Commun. Heat Mass Transfer*, 108 (2019), 104275.
- [65] A. Tassaddiq, S. Khan, M. Bilal, T. Gul, S. Mukhtar, Z. Shah, E. Bonyah, Heat and mass transfer together with hybrid nanofluid flow over a rotating disk, *AIP Adv.* 10 (2020), 055317.

- [66] N. Abbas, S. Nadeem, M. Y. Malik, Theoretical study of micropolar hybrid nanofluid over Riga channel with slip conditions, *Physica A: Stat. Mech. Appl.* 551 (2020), 124083.
- [67] T. Tayebi, H. F. Öztop, Entropy production during natural convection of hybrid nanofluid in an annular passage between horizontal confocal elliptic cylinders, *Int. J. Mech. Sci.* 171 (2020), 105378.
- [68] I. Waini, A. Ishak, I. Pop, Transpiration effects on hybrid nanofluid flow and heattransfer over a stretching/shrinking sheet with uniform shear flow, *Alexandria Eng. J.* 59 (2020), 91-99.
- [69] A. Bhattad, J. Sarkar, P. Ghosh, Experimentation on effect of particle ratio on hydrothermal performance of plate heat exchanger using hybrid nanofluid, *Appl. Therm. Eng.* 162 (2019), 114309.
- [70] M. A. Sadiq, The impact of monocity and hybridity of nanostructures on the thermal performance of Maxwellian thin-film flow with memory and Darcy–Forchheimer effects, *J. Therm. Anal. Calorimetry*, (2020).
- [71] S. Salman, A. A. Talib, S. Saadon, M. H. Sultan, Hybrid nanofluid flow and heat transfer over backward and forward steps: A review, *Powder Technol.* 363 (2020), 448-472.
- [72] G. Humenic, A. Humenic, Entropy generation of nanofluid and hybrid nanofluid flow in thermal systems: A review, *J. Mol. Liquids*, 302 (2020), 112533.
- [73] C. Yildiz, M. Arıcı, H. Karabay, Comparison of a theoretical and experimental thermal conductivity model on the heat transfer performance of Al<sub>2</sub>O<sub>3</sub>-SiO<sub>2</sub>/water hybrid-nanofluid, *Int. J. Heat Mass Transfer*, 140 (2019), 598-605.
- [74] S. Devi, S. Devi, Numerical investigation of hydromagnetic hybrid Cu-Al<sub>2</sub>O<sub>3</sub> water nanofluid flow over a permeable stretching sheet with suction, *Int. J. Nonlinear Sci. Numer. Simul.* 17 (2016), 249-257.
- [75] C. Uysal, E. Gedik, A. J. Chamkha, A numerical analysis of laminar forced convection and entropy generation of a diamond-Fe<sub>3</sub>O<sub>4</sub>/water hybrid nanofluid in a rectangular mini channel, *J. Appl. Fluid Mech.* 12, (2019), pp. 391-402.
- [76] H. Xie, B. Jiang, B. Liu, Q. Wang, J. Xu, F. Pan, An Investigation on the Tribological Performances of the SiO<sub>2</sub>/MoS<sub>2</sub> Hybrid Nanofluids for Magnesium Alloy-Steel Contacts, *Nanoscale Res. Lett.* 11 (2016), 329.
- [77] A. A. Hussien, M. Yusop, W. Al-Kouz, E. Mahmoudi, M. Mehrali, Heat transfer and entropy generation abilities of MWCNTs/GNPs hybrid nanofluids in microtubes, *Entropy*, 21 (2019), 1-17.
- [78] S. Das, R. N. Jana, O. D. Makinde, MHD Flow of Cu-Al<sub>2</sub>O<sub>3</sub>/Water Hybrid Nanofluid in Porous Channel: Analysis of Entropy Generation, *Defect Diffusion Forum*, 377 (2017), 42-61.
- [79] M. Afrand, K. N. Najafabadi, M. Akbari, Effects of temperature and solid volume fraction on viscosity of SiO<sub>2</sub>-MWCNTs/SAE40 hybrid nanofluid as a coolant and lubricant in heat engines, *Appl. Therm. Eng.* 102 (2016), 45-54.
- [80] S. S. Ghadikolaei, M. Yassari, H. Sadeghi, K. Hosseinzadeh, D. D. Ganji, Investigation on thermo-physical properties of TiO<sub>2</sub>-Cu/H<sub>2</sub>O hybrid nanofluid transport dependent on shape factor in MHD stagnation point flow, *Powder Technol.* 322 (2017), 428-438.
- [81] S. S. Harandi, A. Karimipour, M. Afrand, M. Akbari, A. D'Orazio, An experimental study on thermal conductivity of F-MWCNTs-Fe<sub>3</sub>O<sub>4</sub>/EG hybrid nanofluid: Effects of temperature and concentration, *Int. Commun. Heat Mass Transfer*, 76 (2016), 171-177.

- [82] M. H. Esfe, S. Wongwises, A. Naderi, A. Asadi, M. R. Safaei, M. Dahari, A. Karimipour, Thermal conductivity of Cu/TiO<sub>2</sub>-water/EG hybrid nanofluid: Experimental data and modeling using artificial neural network and correlation, *Int. Commun. Heat Mass Transfer*, 66 (2015), 100-104.
- [83] D. Huang, Z. Wu, B. Sunden, Effects of hybrid nanofluid mixture in plate heat exchangers, *Exper. Therm. Fluid Sci.* 72 (2016), 190-196.
- [84] M. Sheikholeslami, S. Mehryan, A. Shafee, M. A. Sheremet, Variable magnetic forces impact on magnetizable hybrid nanofluid heat transfer through a circular cavity, *J. Mol. Liquids*, 277 (2019), 388-396.
- [85] I. Shahzadi, S. Bilal, A significant role of permeability on blood flow for hybrid nanofluid through bifurcated stenosed artery: Drug delivery application, *Computer Meth. Programs Biomed.* 187 (2020), 105248.
- [86] S. Akilu, A. T. Baheta, M. A. M.Said, A. A. Minea, K. V. Sharma, Properties of glycerol and ethylene glycol mixture based SiO<sub>2</sub>-CuO/C hybrid nanofluid for enhanced solar energy transport, *Solar Energy Mater. Solar Cells*, 179 (2018), 118-128.
- [87] R. Mohebbi, S.Mehryan, M. Izadi, O. Mahian, Natural convection of hybridnanofluids inside a partitioned porous cavity for application in solar power plants, *J. Therm. Anal. Calorimetry*, 137 (2019), 1719–1733.
- [88] R. K. Singh, A. K. Sharma, A. R. Dixit, A. K. Tiwari, A. Pramanik, A. Mandal, Performance evaluation of alumina-graphene hybrid nano-cutting fluid in hard turning, *J. Cleaner Product.* 162 (2017), 830-845.
- [89] A. Sidik, I. M. Adamu, M. M. Jamil, G. Kefayati, R. Mamat, G. Najafi, Recent progress on hybrid nanofluids in heat transfer applications: A comprehensive review, *Int. Commun. Heat Mass Transfer*, 78 (2016), 68-79.
- [90] V. Kumar, J. Sarkar, Experimental hydrothermal characteristics of mini channel heat sink using various types of hybrid nanofluids, *Adv. Powder Technol.* 31 (2020), 621-631.
- [91] I. Kazemi, M. Safid, M. Afrand, A novel comparative experimental study on rheological behavior of mono & hybrid nanofluids concerned graphene and silica nano- powders: Characterization, stability and viscosity measurements, *Powder Technol.* 366 (2020), 216-229.
- [92] K. Martin, A. Sözen, E. Çiftçi, H. M. Ali, An Experimental Investigation on Aqueous Fe–CuO Hybrid Nanofluid Usage in a Plain Heat Pipe, *Int. J. Thermophys.* 41 (2020), 135.
- [93] S. S. Botha, P. Ndungu, B. J. Bladergroen, Physicochemical Properties of Oil-Based Nanofluids Containing Hybrid Structures of Silver Nanoparticles Supported on Silica, *Ind. Eng. Chem. Res.* 50 (2011), 3071–3077.
- [94] S. Shaw, Impact of Cattaneo-Christov heat flux on  $\text{Al}_2\text{O}_3\text{-Cu/H}_2\text{O-(CH}_2\text{OH)}_2$  hybrid nanofluid flow between two stretchable rotating disks, Springer Book (Energy Systems and Nanotechnology) *Advances in Sustainability Science and Technology* (2021).